IOPscience iopscience.iop.org

Home Search Collections Journals About Contact us My IOPscience

Physics and tribology of chemical mechanical planarization

This article has been downloaded from IOPscience. Please scroll down to see the full text article.

2008 J. Phys.: Condens. Matter 20 225011

(http://iopscience.iop.org/0953-8984/20/22/225011)

View the table of contents for this issue, or go to the journal homepage for more

Download details:
IP Address: 129.252.86.83
The article was downloaded on 29/05/2010 at 12:30

Please note that terms and conditions apply.

J. Phys.: Condens. Matter **20** (2008) 225011 (13pp) doi:10.1088/0953-8984/20/22/225011

Physics and tribology of chemical mechanical planarization

Toshi Kasai[1] **and Bharat Bhushan**[2,3]

[1] Cabot Microelectronics, 870 North Commons Drive, Aurora, IL 60504, USA
[2] Nanotribology Laboratory for Information Storage and MEMS/NEMS, The Ohio State University, 201 West 19th Avenue, Columbus, OH 43210, USA

E-mail: bhushan.2@osu.edu

Received 1 August 2007, in final form 19 November 2007
Published 30 April 2008
Online at stacks.iop.org/JPhysCM/20/225011

Abstract
The physical and tribological attributes of the chemical mechanical planarization (CMP) process are reviewed. Kinematic analysis of a CMP polisher is described, which can be applied in establishing tribological models. These models elucidate the lubrication regimes at the workpiece/polishing pad interface at the macroscale in order to examine the regional uniformity in the amount of material removed. At the micro/nanoscale, the material removal and planarization mechanisms are mainly discussed from the theoretical and modeling perspective together with experimental verification provided using scanning probe microscopy (SPM) techniques. Selected CMP applications in the field of micro/nanoelectromechanical system (MEMS/NEMS) are also highlighted in conjunction with fabrication processes and tribological challenges at the sub-nanometer scale.

1. Introduction

Incorporation of the chemical mechanical planarization (CMP) technique into the fabrication process of large scale integrated circuits (ICs), ushered in a new era of polishing technology (Kaanta *et al* 1991). The technique enabled the planarization of topographical steps created on IC wafers. This capability allowed the construction of multilevel interconnection structures with a more regularly stacked sequence, resulting in better device performance (Steigerwald *et al* 1997).

A single sided polisher is a common geometry for CMP of an IC wafer (Oliver 2004). The wafer to be polished is supported by a carrier and the wafer/carrier assembly is pushed against a platen through a flexible gimbal joint (figure 1(a)). The surface of the platen is covered with a polymeric pad that transports polishing slurry over the wafer. During polishing, the surface condition of the pad can change; for example the pad material can be degraded and glazed with an absence of sharp asperities, resulting in a reduced removal rate. In order to maintain a consistent polishing performance, a pad is conditioned *in situ* or *ex situ*. As shown in figure 1(a), the *in situ* conditioning is conducted using a conditioning disk with embedded diamond abrasive particles that is swept across the pad surface during polishing. A more microscopic scale view at the wafer/pad interface is shown in figure 1(b). The slurry, that typically contains abrasive particles, oxidant and additives, interacts with the wafer surface, and the slurry chemistry is most likely to modify the surface to a more fragile state. The relative motion between the wafer and the pad allows the pad asperities to drive abrasive particles over the wafer surface. The mechanical abrasion of the chemically modified layer caused by the particles can efficiently achieve material removal and the desired surface finish.

With the need to polish various materials under the demanding requirements of this application, improved process capabilities have been eagerly explored and investigated, primarily on an experimental trial and error basis. An example of this approach is slurry development. Various combinations of component factors, such as types (alumina, silica, ceria), sizes and concentrations of abrasive particles, oxidant (peroxide, acids), various additives (corrosion inhibitor, pH adjuster, complexing agents) and pH have been evaluated based on polishing run results (Oliver 2004). In addition, mechanistic investigations have also been attempted from a theoretical perspective to explain experimental observations and to extend the capability of CMP. Comprehensive modeling and governing equations associated with material removal mechanisms are subsequently scrutinized to find a best known method (BKM).

[3] Author to whom any correspondence should be addressed.

 © 2008 IOP Publishing Ltd Printed in the UK

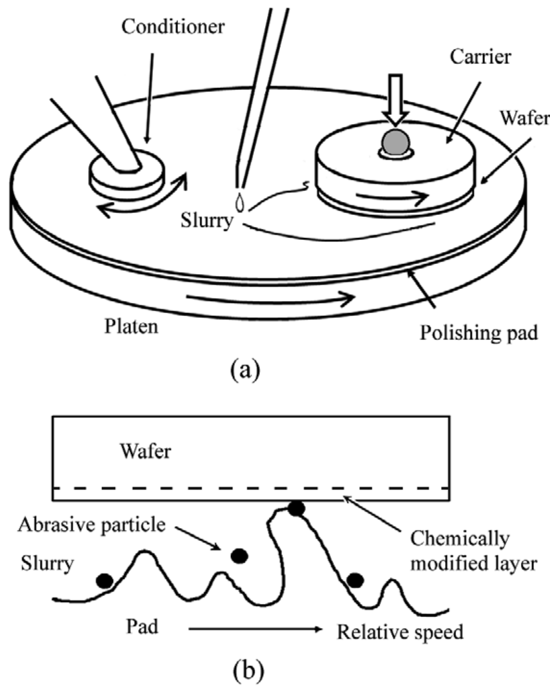

Figure 1. (a) Schematic of the CMP-based polishing process for IC wafers. A wafer attached to a carrier is pushed against a polishing pad. Polishing slurry is provided from the top. *In situ* or *ex situ* conditioning of the pad maintains an optimal pad surface condition during CMP. (b) Illustration of microscopic interaction between the wafer surface and pad asperities in the presence of abrasive particles. Polishing is conducted by the combined action of chemical reactions by the slurry chemicals and mechanical abrasion by the abrasive particles.

One of the more effective approaches to understanding CMP mechanisms is the utilization of tribological concepts and theories, as polishing is an important tribological attribute. Though a main objective in most tribological applications is to reduce friction and minimize wear, e.g. with the use of lubrication techniques (Bhushan 2002), CMP requires a certain amount of material removal while keeping friction and material removal (wear) under control. Recent progress in tribological investigations of CMP has focused on mechanical pad/wafer interactions (Ahmadi and Xia 2001, Castillo-Mejia *et al* 2000, Castillo-Mejia and Beaudoin 2003, Kim *et al* 2003), slurry fluid mechanics (Kim *et al* 2003, Higgs III *et al* 2005, Borucki *et al* 2005), slurry particle abrasion/adhesion (Zhang and Busnaina 1998, Ahmadi and Xia 2001, Luo and Dornfeld 2003, Thagella *et al* 2004) and dynamic thermal behavior (White *et al* 2003, Borucki and Philipossian 2007).

In this paper, physical and tribological approaches for elucidating mechanisms of CMP at different length scales are reviewed. In section 2, tribological investigations at the macroscale are introduced. The kinetics of a single sided polisher is first outlined, in which an analytical technique is described for obtaining the relative velocity and travel distance of a single location on a workpiece under specific kinematic process parameters (Patrick *et al* 1991, Oliver 2004). Then, the Preston equation (Preston 1927), an empirical law which correlates the process variables with material removal rate, is evaluated with experimental results. The mechanistic interpretation of this analysis is also presented. Wafer/pad interface tribology is addressed next. The lubrication regimes, asperity contact and fluid thickness/pressure are examined in conjunction with key contributing factors, such as the properties of the pad, wafer and slurry combined with polisher run conditions. These analyses are used in evaluating the resulting within-wafer non-uniformity in the removal rate. In section 3, the material removal and feature scale step planarization mechanisms are addressed at the micro/nanoscale (Evans *et al* 2003). The Langmuir–Hinshelwood type dynamics model is known to effectively combine chemical and mechanical material removal mechanisms in CMP (Paul 2001, Borucki and Philipossian 2007). Component level analysis/modeling in terms of CMP slurry (Luo and Dornfeld 2004) is highlighted as well as various models and simulations developed for predicting pattern-dependent post CMP surface features based on these mechanisms (Vlassak 2004). Experimental verification using an innovative AFM technique that represents a single asperity interaction is presented. It can provide insight into the microscopic CMP mechanisms to interpret the macroscopic CMP phenomena (Bhushan 1999, DeVecchio *et al* 2000, Berdyyeva *et al* 2003). In section 4, selected topics in CMP applications for MEMS/NEMS (Eaton and Smith 1996, Bhushan 2007) are addressed.

2. Macroscale view of CMP

2.1. Kinematic analysis of a single sided polishing system

Understanding the kinetics of polishers used in CMP is useful for obtaining the desired polishing performance. For IC wafer polishing, single sided polishers are generally used, while double sided polisher/lapping machines are common in rigid disk CMP (Hagihara *et al* 2002, Kasai 2008) and silicon wafer lapping (Ahearne and Byrne 2004). In this section, the focus is on a single sided polishing.

Figure 2 shows a selected region of a single sided polisher, viewed from the top, containing a wafer attached to a carrier and to a part of the platen. Using the geometrical notations in figure 2, the relative velocity at a given location on a wafer is considered. The x–y coordinate system can be set as shown in the figure and then the origin is found at the center of the platen, denoted as O. The distance between the centers of the platen and the carrier, the latter denoted as O', is b. The angular velocities of the carrier and the platen are ω_1 and ω_2, respectively. Both are rotated in the counter-clockwise direction. It is assumed that the wafer is attached to the carrier firmly so that no sliding occurs between the carrier and the wafer. The location of interest, P, on the wafer has a distance of r_1 measured from O' and r_2 from O, and $O'P$ and OP make an angle θ and ϕ, respectively, with the x-axis. Originally, at time equal to zero, the location was on the x-axis, and at the time t, the location moves to P in the figure. The x–y coordinates of P can be described as

$$x = r_1 \cos\theta + b = r_2 \cos\phi \qquad (1)$$

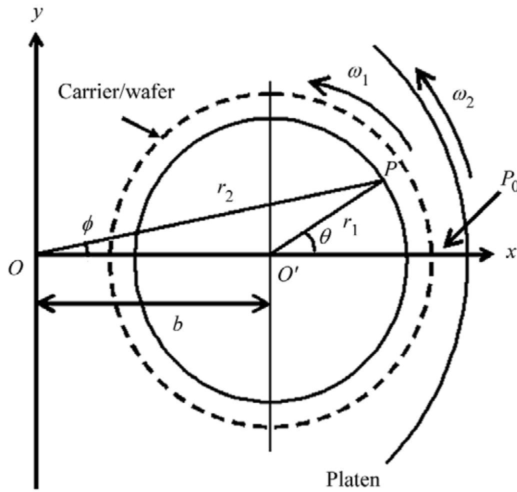

Figure 2. Top view of a single sided IC wafer polisher. The geometry includes a carrier and part of a platen.

$$y = r_1 \sin\theta = r_2 \sin\phi. \tag{2}$$

The relative velocity, v, is the velocity of the wafer with respect to that of the pad. From equations (1) and (2) and geometrical settings, the x and y components of v are

$$v_x = -r_1(\omega_1 - \omega_2)\sin\omega_1 t \tag{3}$$

$$v_y = r_1(\omega_1 - \omega_2)\cos\omega_1 t - \omega_2 b. \tag{4}$$

Note that in the case of an equal rotation speed for the carrier and platen, the relative velocity is independent of time and location when the two process parameters, ω_2 and b, are held constant (Patrick *et al* 1991). The relative speed is the magnitude of the velocity, and is described as

$$\overline{v} = \sqrt{v_x^2 + v_y^2}. \tag{5}$$

A friction force is generated when two surfaces have a relative motion. The direction of the force is opposite to that of the velocity, and can be expressed as

$$F_{\text{friction}} = -\mu \overline{N} \frac{v}{\overline{v}} \tag{6}$$

where μ is the coefficient of friction and N is the down force. The friction force is usually measured as a force generated on the axis at the center of the carrier. This is an integrated force exerted on the elements of the whole carrier surface. Thus, the averaged friction force integrated around the carrier center is given by

$$F_{\text{averaged friction}} = \frac{1}{S}\oint F_{\text{friction}}\,\mathrm{d}s \tag{7}$$

where ds is the area of a small element and S is the total area of the wafer in contact. It should be noted that the velocity and the normal pressure can be location dependent. For example, the relative velocity depends on the rotation speed of the carrier and the platen as suggested by equations (3) and (4). Also, a flexible gimbal joint on top of the carrier (see figure 1(a)) allows a tilt of the wafer toward the leading edge due to friction. This geometry is detailed in 2.3. With

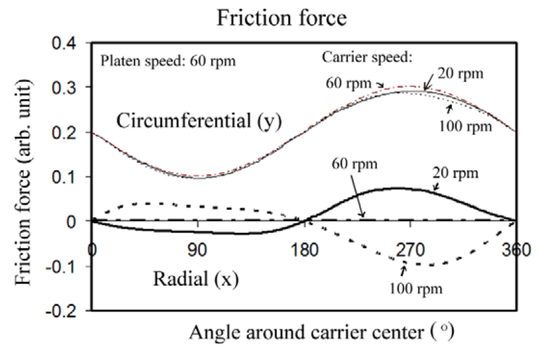

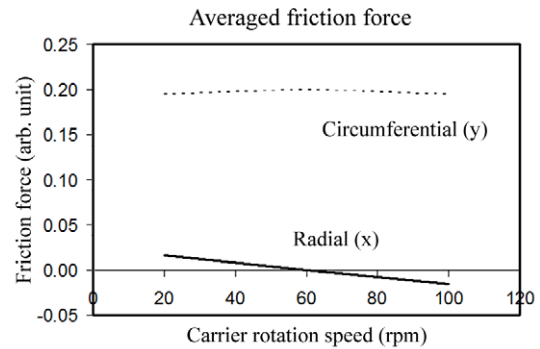

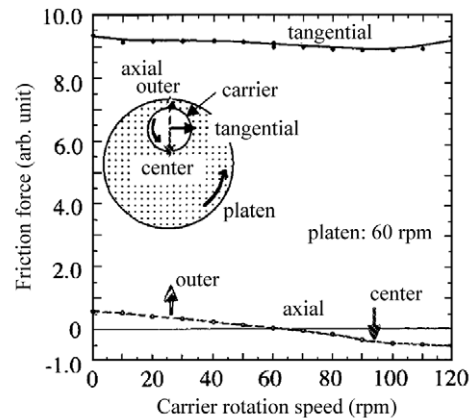

Figure 3. (a) Radial and circumferential components of the friction force calculated using the analysis at different angular locations along the carrier center for three carrier rotation speeds. (b) Dependency of the friction force on carrier rotation speed. (c) Experimental results supporting the analysis. Part (c) is reproduced by permission of the Electrical Chemical Society (Homma Y *et al* 2003 *J. Electrochem. Soc.* **150** G751–7).

the consideration of these effects, the radial (x-direction in figure 2) and the circumferential (y-direction) components of the friction force exerted at the location P on the wafer were calculated. Figure 3(a) shows the radial and circumferential components of the friction force versus an angle around the carrier center at a fixed radial location. The angle is set to be zero at time equal to zero and increases in the counter-clockwise direction (see figure 2). Three cases are shown: the rotation speed of a carrier smaller than (20 rpm), equal to (60 rpm) and larger (100 rpm) than that of a platen (60 rpm). The phase of the radial friction force becomes opposite,

depending on which speed is larger, the carrier speed or the platen speed. This occurs due to the terms ω_1 and ω_2 in equation (3). On the other hand, the circumferential component is not much affected. As a result, as shown in figure 3(b), an averaged friction force exerted at the carrier center with a fixed platen rotation speed (60 rpm) shows a sign conversion in the radial friction when the carrier rotation speed is changed. This result is consistent with the experimental evidence reported by Homma *et al* (2003). They developed a monitoring system capable of measuring a radial (axial in the figure) friction as well as a circumferential (tangential) friction. It was found that an axial component of the friction force had a dependency on the carrier speed relative to the platen speed (figure 3(c)). When the carrier speed was smaller than the platen speed, the axial friction component pointed in a direction away from the carrier center toward the edge, and vice versa.

The case discussed above is for a polishing head design with a flexible ball joint gimbal system. Taking this design to an extreme is the joint design equipped with a spherical surface that has a concave curvature. This design allows a projected gimbal point to be situated below the wafer surface so that the wafer is forced into a leading edge up geometry on the pad (Halley 2003). The friction force profiles could be completely different using this design.

Some polishers are designed to operate with an oscillation motion of a carrier along the radial direction. The analysis shows that the contribution of oscillatory motion to the relative velocity is small since the oscillation frequency (typically ~0.5 rpm) is much smaller than that of carrier rotation speed (~60–130 rpm). The main objective for the use of oscillatory motion is to utilize more pad area in polishing.

2.2. The Preston equation

Though various innovative improvements have been made in the components of polishers, e.g. the head designs and polishing pad structures, the basic configuration is the same as that long used for glass polishing. For early investigators, prediction of the amount removed in conjunction with process parameters was an important issue. Preston (1927) proposed an empirical equation that describes the relationship between the polishing rate of glass, the normal pressure and the polishing speed

$$w = k_P p v t \tag{8}$$

where w is the amount removed in time t, k_P is the Preston coefficient, p is the nominal pressure and v is the linear relative speed. The polishing rate, w/t, is typically used as a key output parameter. Later investigators found this equation to be valid for other materials, though some modifications were proposed based on the material being polished (Oliver 2004, Paul *et al* 2005). As a result, the Preston equation has been commonly used in the industry. In this application, the term k_P is interpreted as a representation of other contributing factors such as chemical effect and geometrical factors.

In the field of tribology, Holm and later Archard (1953, 1977) introduced the wear equation for unlubricated sliding (Bhushan 2002):

$$W_{\text{volume}} = \frac{k_A}{3}\frac{N}{P_m} l_{\text{sliding}} \tag{9}$$

where W_{volume} is the wear volume, k_A is the Archard coefficient, N is the applied normal load, P_m is the yield strength of a more compliant material in contact and l_{sliding} is the sliding distance. The equation was derived based on adhesive contact theory, which requires that material hardness be incorporated. What the two equations suggest is essentially the same thing (Hutchings 2002). This is understandable considering that the Preston equation was used for the wear of glass for which the polishing mechanism is dominated by mechanical action. For a more general case, in which the velocity changes with time, the Preston equation can be modified, assuming k_p and p are constant during polishing, to a form similar to the Archard equation:

$$w = k_P p \int v \, dt = k_P p L \tag{10}$$

where w is the amount removed, typically measured by the reduction in thickness or weight, and L is the travel distance, corresponding to l_{sliding} in equation (9).

The kinematic model mentioned earlier showed that the travel distance is not significantly affected by the change in the carrier speed, but by the platen speed, due to the second term in equation (4). From equation (10), the amount of material removed can be proportional to the travel distance. In order to confirm this analysis, the following polishing runs were conducted. The CMP polishing tester (Universal Bench Top Tribometer, CETR Corp.) was used for polishing rigid disk samples (95 mm outer diameter) for 60 s with a silica and peroxide based slurry (EP-DSK 7000 A40, Cabot Microelectronics). The amount of material removed was evaluated as the weight change before and after polishing. Figure 4 shows the travel distance calculated and the amount of material removed as experimentally observed under the condition that either the speed of the carrier (a) or the platen (b) was varied, while the other was kept constant. The trend between the travel distance and the amount of material removed is consistent. As seen in figure 4(a), the carrier speed does not influence the amount of material removed in the range studied. As the carrier speed becomes larger than the range, the effect of frictional heating becomes more significant and then the amount removed may increase with the carrier speed.

More fundamental mechanistic approaches have been attempted to re-examine the correlation among the parameters of the Preston equation. Examples are an elastic material model (Brown *et al* 1981), asperity contact models (Yu *et al* 1993, Ahmadi and Xia 2001) and erosion models (Runnels and Eyman 1994, Sundararajan *et al* 1999, Sukharev 2001). These models all give rise to a governing equation similar to the Preston equation. The Preston coefficient has been represented using parameters to incorporate various effects. It has also been observed, however, that the linearity described in the Preston equation is not always valid. A linear relationship between polishing rate and pressure is generally found; on the other hand, polishing rate and velocity are not always related linearly (Hocheng *et al* 2001). This has been attributed to changes in temperature and strain rate when the velocity changes (Rigney 1988, Karthikeyan *et al* 2005). Modified equations have been proposed with non-linear terms in pressure and speed

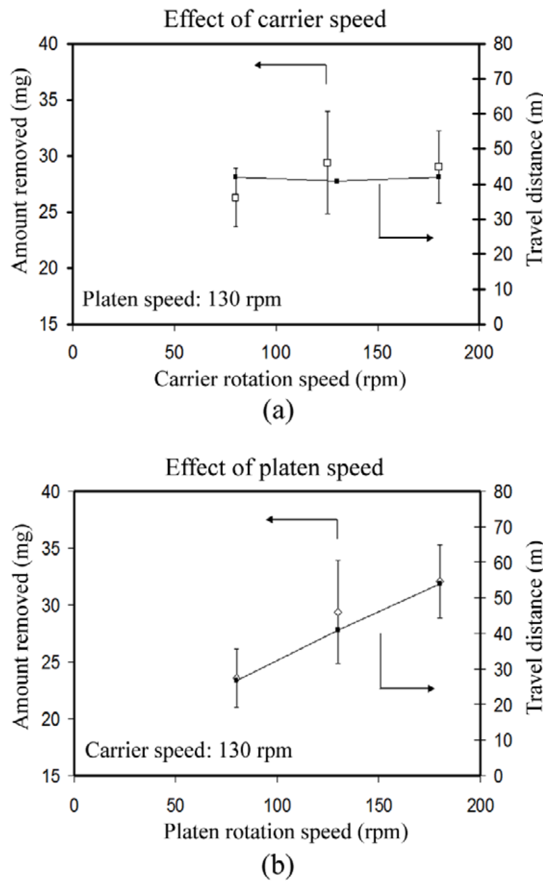

Figure 4. Calculated travel distance and the amount of material removed versus rotation speeds of (a) the carrier and (b) the platen.

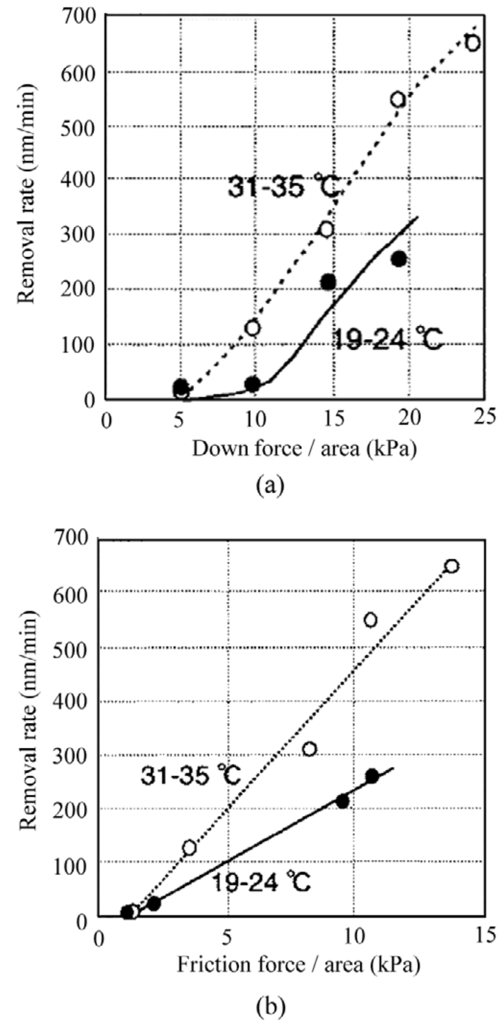

Figure 5. Removal rate versus (a) down force per unit area and (b) friction force per unit area under different temperatures of a pad using abrasive-free slurry for Cu CMP. Reproduced by permission of the Electrical Chemical Society (Homma Y 2006 *J. Electrochem. Soc.* **153** G587–90).

(Tseng *et al* 1999, Hocheng *et al* 2001), appropriate to a given combination of materials, slurry fluid, environment, geometry and process (Luo *et al* 1998). Difficulties in the identification of such parameters make the development of predictive models very challenging (Evans *et al* 2003).

In general, friction and wear are not correlated, possibly because friction is affected by all the interaction events that are produced by the asperity contact between the two surfaces, while material removal (wear) results from a much smaller portion of such events (Archard 1977). It can be also noted that even though material fracture occurs during sliding, wear may not be observed. An example is the wear rate in a vacuum, which can be appreciably lower than that in air, because wear debris is likely to stick to the surface without detachment (Rigney 1997). However, under some specific conditions, a reasonable correlation between friction and wear may be found. Homma (2006) used a concept similar to the energy based friction model established by Heilmann and Rigney (1981) to represent the wear from the viewpoint of energy conservation. It was pointed out that the work input during polishing contributes to the material removal and under those conditions wear should be related to the polishing rate. Macroscopically, the work invested is the product of a drag (friction) force and a sliding distance. Therefore the coefficient of friction (μ) can be incorporated into the Preston equation denoted as

$$w/t = k_{\mathrm{P}}\mu P v + c \tag{11}$$

where c is a constant. In typical CMP processes, the coefficient of friction is in a restricted range (∼0.3–0.7); therefore the incorporation of μ in the equation is not expected to have a significant effect. However, some data confirm the predictions of equation (11). Figure 5 represents the removal rate plotted versus down force per unit area in (a) and friction force per unit area in (b) (Homma 2006). Copper wafers were polished with the use of abrasive-free slurry at different temperatures (18–24 and 31–35 °C). As shown, the plot with friction force demonstrates a well-behaved linear relationship with the removal rate suggested by equation (11), as compared to that for contact pressure. At lower temperature, the protective layer on the wafer surface, formed with the aid of benzotriazole (BTA) in the slurry, prevented abrasion at some portions by the formation of protective layers; on the other hand, at higher temperature, the material removal was possibly more enhanced due to initiation by each pad asperity contact.

2.3. Tribological analysis of pad/wafer interface

To analyze the steady state lubrication condition in CMP, theories established in tribology such as fluid and contact mechanics have been applied. The measured coefficient of friction suggests that the lubrication regime at the wafer/pad interface is boundary lubrication, as denoted in the Stribeck curve (Bhushan 1996a). This is further confirmed by the observation that the estimated fluid film thickness is of a similar order as the pad roughness (Tichy *et al* 1999, Lawing 2002), which is a criterion of boundary lubrication. In this regime, the fluid film pressure is not enough to totally separate a wafer from the pad surface, leading to more pad asperity (solid/solid) contact in supporting the applied normal load (Bhushan 2002, Kim *et al* 2003, Scarfo *et al* 2005).

As discussed in 2.1, the kinematic analysis showed a uniform relative speed across the wafer at a constant speed for the co-rotating carrier and platen. This simplifies the analysis, because according to the Preston equation the factor affecting the polish rate is pressure only, when the Preston coefficient and the speed are kept constant. Taking advantage of this configuration, the local distributions of a normal force at the wafer edges in conjunction with pad properties were calculated using the finite element method (FEM) and yield stress theory for conformal contact. The wafer non-uniformity in the removal rate (Wang *et al* 1997, Castillo-Mejia and Beaudoin 2003) and the effect of a retaining ring (Castillo-Mejia *et al* 2000) were examined. A retaining ring is an additional supporting element located at the circumference of the wafer in order to mediate edge non-uniformity.

For more general microscopic simulations, the uniform relative velocity allows one to perform a simplified two-dimensional analysis along the tangential direction from the leading edge to the trailing edge of a wafer in order to examine the variations of properties. Runnels and Eyman (1994) emphasized the importance of applying fluid mechanics to analyze the motion of a wafer over a pad. As shown in figure 6(a), the model assumed a convex wafer curvature and converging geometry of wafer/pad interface from the leading edge to the center of the wafer. Such an analysis has been well studied for various bearing systems based on the Reynolds equation (Hamrock *et al* 2004). The fluid film thickness, a key to characterizing the lubrication regime, was calculated with various parameters, such as relative speed, wafer curvature and viscosity of the fluid. The calculation assumed that the pad had no roughness and the fluid followed Newtonian flow. Jeng *et al* (2003) considered asperity contact based on the Greenwood–Williamson (GW) asperity model (1966) with the addition of a fluid dynamics model to estimate the pressure profiles, separation distance and contact ratio versus factors such as location, speed and particle size in a slurry fluid. The models mentioned above have suggested a converging wafer configuration. This was based on the following assumptions: frictional force associated with pad asperity contact and/or the consideration of a force balance without a moment balance around the gimbal joint were ignored. Even though the experimental evidence and contact analysis have shown that the real contact area can be of the order of less than 1% of the nominal contact area (Bhushan 1996b, Gray *et al* 2007), the friction force generated cannot be ignored. More plausible analyses have been made and these results are discussed next. However, a converging wafer configuration may be possible in the special cases represented by the use of a wafer with a convex curvature, a lower pressure, a larger relative speed and a very smooth pad (Bullen *et al* 2000, Scarfo *et al* 2005).

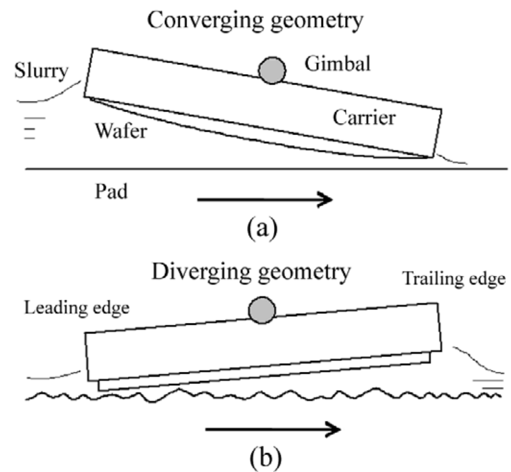

Figure 6. Schematic of the wafer/pad interface at steady state motion of a polishing wafer/carrier assembly (head) with (a) converging and (b) diverging polishing carrier/wafer assembly geometry.

Tichy *et al* (1999) assumed a simplified geometry for pad asperities. They considered regularly aligned pad asperities contacting a wafer. Two types of pad deformation were considered to collectively originate from the deformation of each asperity and a bulk pad material. The latter was called a 'mattress effect'. The fluid film thickness was estimated to be equivalent to the height of the deformed asperities. The authors extended this approach by introducing a more realistic GW asperity model and made an analysis based on a force and moment balance (Kim *et al* 2003). Their results showed that the polishing head diverged from the leading edge to the trailing edge caused by friction (figure 6(b)). Due to this head diverging effect, total asperity deformation is expected to be larger at the leading edge than at the trailing edge. Experimental evidence measured on the vertical head movement supported this head-diverging geometry (Ng *et al* 2004, Lu *et al* 2004). A negative fluid pressure (suction) near the leading edge and a positive pressure at the trailing edge due to the pad deformation together with the head tilt were suggested (Higgs III *et al* 2005, Borucki *et al* 2005). Also, the fluid pressure distribution was found to be significantly affected by the rotation of a carrier (Bullen *et al* 2000).

In summary, each model emphasizes different lubrication regimes. Judging from the coefficient of friction, mixed or boundary lubrication is most likely to occur in CMP. The force and moment balance analysis suggests that head-diverging geometry for a wafer with respect to the pad surface is most plausible.

3. Micro/nanoscale aspects of CMP mechanisms

3.1. Material removal mechanisms and feature scale planarization modeling

The material removal mechanisms are dependent on the chemical nature of the surface being polished. In the CMP of IC wafers, dielectrics and metals are two major materials to be polished. Dielectrics are made typically of silicon dioxide, and low-k dielectrics are being explored for next generation IC applications. Metals include tungsten, copper, tantalum and aluminum. Material removal mechanisms and associated modeling are highlighted in this section.

A silicon dioxide layer can be deposited by chemical vapor deposition (CVD) of a gaseous compound, tetraethyl orthosilicate (TEOS: $Si(OC_2H_5)_4$). The CMP of TEOS based oxide layers is analogous to traditional glass polishing. Cook (1990) gave a mechanistic explanation of silicate glass polishing in which chemical aspects were emphasized. The water in a polishing fluid interacts with the glass to form hydroxyl groups on the glass surface. Mechanical forces exerted by pad asperities on the glass surface, possibly through abrasive particles, can enhance this reaction. This reaction can lead to bridge formation (Si–O–M) between the glass and the abrasive particles, allowing the detachment of the glass material. Moreover, the slurry for silicon dioxide CMP is typically maintained at a higher pH, which can accelerate the chemical reaction by softening the surface. Mechanical abrasion of the modified surface layer is also attributed as part of the removal process. Abrasives driven by asperities of a pad primarily interact with topographically elevated regions of the wafer to be removed, so that better planarization is achieved. In addition, the high-pH environment is advantageous since silica abrasive particles are well dispersed.

In metal CMP, chemical reactions near the wafer surface play a more dominant role. The surface is chemically modified by oxidants in the CMP slurry and transformed to more easily removed compounds. In tungsten CMP, Kaufman *et al* (1991) suggested a passivation reaction of tungsten in a slurry environment, forming a softer tungsten oxide layer as suggested by the reaction equation

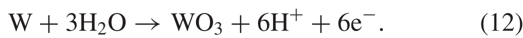

$$W + 3H_2O \rightarrow WO_3 + 6H^+ + 6e^-. \quad (12)$$

The oxide layer is removed by the mechanical force exerted by abrasives. The material removal is enhanced through the use of complexing agents that produce water soluble compounds with abraded materials (Patri *et al* 2005). It can be noted that the oxidation state of the surface depends on the chemical environment (Oliver 2004).

Paul (2001) used Langmuir isotherm type dynamics (Hinshelwood 2005, Borucki and Philipossian 2007) to analyze the tungsten CMP in a two-step material removal process, chemical reaction (oxidation) followed by mechanical abrasion:

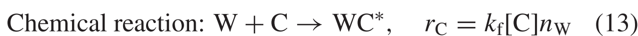

$$\text{Chemical reaction: } W + C \rightarrow WC^*, \quad r_C = k_f[C]n_W \quad (13)$$

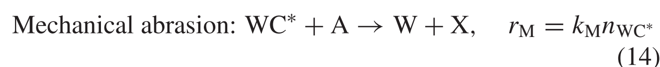

$$\text{Mechanical abrasion: } WC^* + A \rightarrow W + X, \quad r_M = k_M n_{WC^*} \quad (14)$$

where C is the oxidizer, WC* is the complex tungsten oxide, A is the abrasive particle, X is the compound of tungsten oxide and an abrasive particle, r_C is the rate of the oxidation per unit time and area, k_f is the chemical reaction rate constant, [C] is the concentration of the oxidizer, n_W is the tungsten concentration on the surface, r_M is the mechanical removal rate of the oxide, k_M is the mechanical proportionality constant and n_{WC^*} is the concentration of the complex oxide on the surface. The effect of temperature can be incorporated into the term, k_f (Hocheng *et al* 1999). Two equations were additionally given:

$$r_C = r_M \quad (15)$$

$$n_W + n_{WC^*} = 1. \quad (16)$$

Equation (15) represents the steady state condition in which the apparent concentration of tungsten oxide on the surface is independent of time. Equation (16) is based on the assumption that the surface consists of either tungsten or tungsten oxide, with a removal rate given by

$$RR = \tau k_M n_{WC^*} = \frac{\tau k_M k_f [C]}{k_f [C] + k_M} \quad (17)$$

where RR is the removal rate and τ is the thickness of the removed film times the workpiece area. The final form of equation (17), derived using equations (15) and (16), demonstrates that at a high concentration of oxidizer or a large $[C]$, the mechanical term (k_M) is the rate determining factor and at large mechanical removal conditions the process is limited by chemical reaction (Evans *et al* 2003). To evaluate k_M, a Preston-style equation was used, in which the size and concentration of abrasive particles and asperity contact information were included so that the effect of process parameters such as velocity and pressure was considered.

For metals that are more chemically active, such as copper, a corrosion inhibitor, e.g. BTA, is generally added in the slurry to protect topographically recessed regions from excessive etching and mechanical abrasion (Kim *et al* 2005). This promotes planarization efficiency due to the reduced removal rate at the topographically recessed regions. Paul and Vacassy (2003) extended their model to incorporate the effect of inhibitors by adding a term for the concentration of inhibitor molecules in equation (16). In addition, a three-step process was introduced with an additional chemical reaction (Paul *et al* 2005), since copper has two oxidation states, CuO and Cu_2O, depending on the environment (Aksu *et al* 2003). The removal rate showed a local peak with the concentration of peroxide, a typical oxidizer used for metal CMP, due to the different oxidation states yielding distinct levels of polishing performance. The model successfully explained the removal rate performance of the slurry.

Perhaps one can consider the polishing slurry to be the most important component in CMP (Xie and Bhushan 1996a). As aforementioned, slurry consists normally of de-ionized water, abrasive particles, an oxidizer, complexing agents and other chemical additives, such as a pH modifier. Various factors such as particle type, particle size, per cent solid loading and pH affect the polishing performance (Xie and Bhushan 1996b, Luo and Dornfeld 2003, 2004, Oliver 2004,

Remsen *et al* 2006). Luo and Dornfeld (2003) focused on active particles, which confirm the size with the clearance between the pad asperities and the wafer surface. They established a model that showed a correlation between the particle size and the removal rate. Ahmadi and Xia (2001) used contact mechanics (Johnson 1985) to calculate the real area of contact for soft/hard pads and different slurry concentration geometries, and applied an adhesion and abrasion wear model to estimate the penetration depth of abrasive particles into the wafer surface and the removal rate. This model predicted a monotonic increase in penetration depth and a decrease in the removal rate with a larger particle size. This approach also gives some insight into the process of creating scratch defects depending on the properties of the pad material. It is well known that the use of a softer pad results in fewer scratch defects than a harder pad, though surface planarization produced by a hard pad is superior.

The microscopic material removal models described above have been used to predict the feature scale material removal process of patterned wafers. Models for step height reduction and associated dishing and erosion have also been discussed. Dishing is a metal line recess with respect to the surrounding oxide and erosion is a material loss of oxide at metal/oxide mixed line patterns. Both issues lead to an unbalanced material removal rate affected by the geometrical effects and the material properties, and significantly deteriorate the surface planarity, known to be major challenges in the CMP of patterned IC wafers. It is empirically recognized that during the planarization of steps created on a homogeneous material surface, material removal depends on the geometrical structures of the steps. For example, small and positive steps experience more aggressive material removal than large and negative steps. Warnock (1991) proposed that the dependency of variations in removal rate on the topography is mainly induced by conformal pad contact, and then presented a model expressing the dependence of the removal rate on the topographical profiles for different sizes and pattern densities. Runnels (1994) used a hydrodynamic fluid flow model described earlier for evaluating the material removal by erosion. This model estimated local stresses at topographical steps to predict the planarization rate. Sundararajan *et al* (1999) proposed a model similar to that of Runnels for Cu polishing. The model assumed that the material removal was driven by chemical reaction and limited by the diffusion of by-products. The mass transport equation was solved to obtain an average polish rate as a function of various factors, including Cu flux, slurry composition and particle distribution. Sukharev (2001) introduced the concept of etch pit nucleation–propagation for a material removal process based on dissolution kinetics. This model provided an equation for removal rate in conjunction with pressure and dimensions of the area polished to estimate dishing and erosion.

For surface regions that consist of multiple materials, modeling tends to be more complicated due to the polishing rate selectivity. Recent analyses have successfully correlated the dishing and erosion with various process parameters during polishing (Vlassak 2004, Guo *et al* 2004). In these models, the variations in local stress are used to calculate the planarization efficiency of finished surfaces, derived from the Preston equation. Simulations using the finite element method (FEM) and/or boundary element method (BEM) have been also conducted to examine multiscale stress distributions (Yoshida 2005).

3.2. AFM technique for simulating asperity contact

The advancement of the AFM technique with associated data interpretation methods and contact models has been significant in the investigation of tribological issues at the micro/nanoscale (Bhushan 1999, 2005a, 2005b, 2007, Kim and Bhushan 2006). These techniques, together with the fluid cell attachment capability to an AFM, allows experimental examinations of fundamental aspects of CMP processes. As discussed earlier, at the micro/nanoscale, pad asperities are in contact with a wafer surface either directly or through abrasive particles (see figure 1(b)). An abrasive particle pushed against a wafer surface by a pad can be simulated by an AFM tip scanned along a sample surface at a controlled force in a fluid environment in order to investigate the asperity scale dynamics (DeVecchio *et al* 2000, Stevens *et al* 2003).

Several key features of this technique are described as follows: the nominal tip radius is of the same order as the size of the abrasive particle. The normal load exerted on an AFM tip can also be maintained at a similar down force expected at a single asperity of a pad during CMP. Both rastering and imaging of the surface can be performed using the same tip. Moreover, associated techniques such as Kelvin probe force microscopy (KPM) can be also applied. Though the typical tip sliding speed is $\sim 30\ \mu\mathrm{m\,s^{-1}}$, which is far smaller than the relative sliding speed commonly seen in the actual CMP process ($\sim 100\ \mathrm{mm\,s^{-1}}$), some effort has been made to compensate for this difference in order to obtain a good estimate in the removal rate (Berdyyeva *et al* 2003). In addition, recent advances allow single phase abrasive particles to be mounted on an AFM cantilever. Using this modified AFM tip, adhesion, friction and wear via the interaction between the particles with desired size and counter materials can be examined in a well controlled environment (Ong and Sokolov 2007).

The physical and chemical properties of two surfaces in a liquid phase, as well as associated structural and chemical changes during interaction of the surfaces, contribute to the interaction forces generated between the surfaces in contact or near contact below a few nanometers. In the case of the AFM tip technique in a CMP environment, the van der Waals attraction is generally reduced, and long-range electrostatic forces and other short-range forces, mainly originating from chemical bonding, will predominate (Bhushan 1999, 2005b). Electrostatic attractive/repulsive interaction forces increase/decrease friction and wear between two surfaces. The charging of particles plays an important role in determining the electrostatic forces generated on the single particle modified AFM tip. A particle mounted on a cantilever generates attractive or repulsive forces when the AFM cantilever is driven vertically toward or against the surface. The forces can be estimated by measuring the deflection of the cantilever (Lin *et al* 1993, Bhushan 1999, Cooper *et al* 2002).

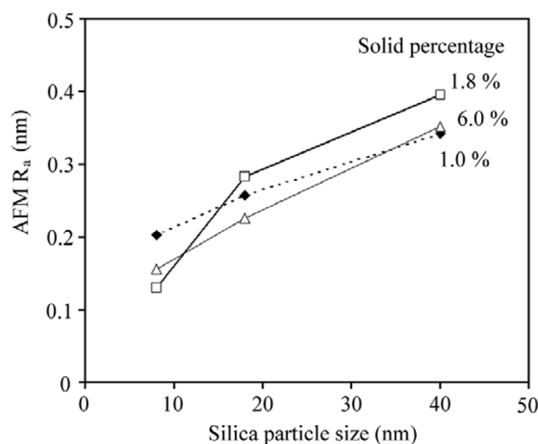

Figure 7. Effect of abrasive particle size on R_a measured by an AFM (AFM R_a). Samples are rigid disks polished using silica based CMP slurries with three different levels of particle concentration (solid%), 1.0, 1.8 and 6.0%. The use of smaller sized particles reduces AFM R_a effectively.

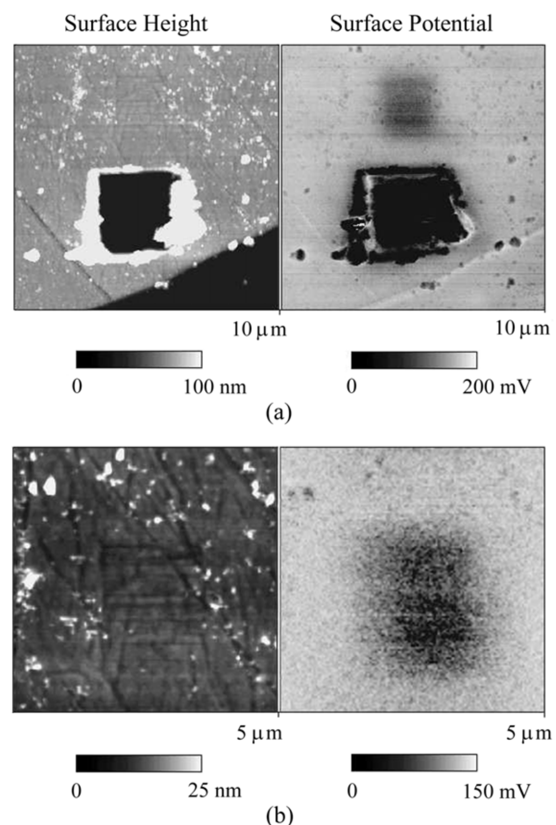

Figure 8. (a) Surface height and surface potential maps of wear regions generated at 1 and 9 μN on a single-crystal aluminum sample. Noticeable change is found in the surface potential but not in the surface height for the worn region under 1 μN load (just above the larger wear mark in square shape). (b) Close-up of the upper (1 μN load) wear region. Reprinted with permission from DeVecchio and Bhushan 1998 *Rev. Sci. Instrum.* **69** 3618–24. Copyright 1998, American Institute of Physics.

Several examples have demonstrated the effectiveness of the AFM technique. Enhanced material removal of deposited aluminum films was seen under rastering by an AFM tip operated in a corrosive chloride solution environment, while noticeable wear was absent in de-ionized water (Chen and Guay 1994). This was attributed to the thinning of the aluminum oxide layer formed in the solution. The surface roughness was also found to decrease with the rastering time. This is consistent with the reduction in roughness typically achieved using the CMP process. Figure 7 shows silica abrasive particle size and arithmetic mean roughness (R_a) measured by an AFM on a $10 \times 10\ \mu m^2$ area, referred to as AFM R_a, of polished Ni-P surface in CMP. Slurries with three different levels of particle concentration (solid%), 1.0, 1.8 and 6.0% were used. Using particles that were tens of nanometers in size, sub-nanometer level surface roughness can be easily achieved. This excellent surface finish can be obtained not only from a mechanical contribution but also from a certain level of chemical reaction which minimizes surface damage during planarization. Chandra and co-workers used molecular dynamics (MD) simulations to model the effect of chemical reactions that contribute to surface roughness (Ye *et al* 2003). The abrasion between an AFM size scale cutting tip and a copper surface was examined. The result indicated that a smooth and defect free surface would result when an AFM tip was swept across the substrate in the presence of chemical dissolution agents.

Schmutz and Frankel (1998) performed AFM scratch tests on aluminum alloy (AA2024-T3) samples. They used a scanning KPM to characterize intermetallic particles. This technique measures the Volta (surface) potential closely related to the difference in the electron work function (EWF) of metals, which indicates the location of particles, even in the topographically flat regions. Immediate dissolution of Al–Cu–Mg particles by rastering with an AFM tip was found in a chloride solution. The dissolution was completely suppressed by the addition of very dilute concentrations of dichromate ($Na_2Cr_2O_7$) (Schmutz and Frankel 1999). An Auger analysis showed that the Al–Cu–Mg particles contained a higher concentration of Cr, suggesting the chemical/structural transformation of the particles. Frankel *et al* extended this technique and examined the effect of down force, potential, pH and oxidizing agents (DeVecchio *et al* 2000). An increased removal rate on an aluminum surface with an increase in down force and pH was found. The presence of an oxidizing agent in the solution had a similar effect on the removal rate (increased) as an applied potential. The findings are consistent with general results observed in macroscopic CMP experiments.

The effectiveness of utilizing the KPM technique in wear study has also been described. The surface potential, emphasized by the technique, can trace the associated chemical and/or structural changes on the surface. DeVecchio and Bhushan (1998) applied this technique to detect early stages of wear. They abraded a polished single-crystal aluminum (100) sample using a diamond tip at loads of 1 and 9 μN, and then scanned the surface with the KPM mode together with the standard surface height AFM mode. As shown in figure 8(a), the surface height map shows a clear wear mark in the region abraded under 9 μN load (a larger square), but no detectable changes in the area scratched under 1 μN (just

above the square). On the other hand, the surface potential map reveals an apparent potential contrast (∼0.17 V) in both regions. Close-up images of the upper (1 μN load) wear region are shown in figure 8(b).

The AFM scratch technique was applied in characterizing a copper surface in a solution that was nearly identical to an actual CMP slurry, studied by Sokolov and co-workers (Berdyyeva *et al* 2003). The sample was immersed in a slurry environment and then replaced with one that did not contain oxidizers. AFM scratch tests were conducted to characterize the mechanical removal process. The removal rate increased with a decrease in pH, which was correlated to the hardness of the surface layer. This finding was consistent with the trend experimentally shown using nano-indentation testing (Jindal *et al* 2001) for Cu surfaces during CMP. The friction force was also measured with an AFM tip and a similar trend to that for the removal rate in certain pH range was also found. This tendency suggests a close correlation between the two parameters, as discussed in 2.2. A comparison was also made between micro and macroscale removal rates. The scaled AFM removal rate was much higher than the estimated copper removal rate per single abrasive particle.

The AFM force calibration plot technique is generally used to investigate adhesion and short/long-range interaction forces between two surfaces (Bhushan 1999). Hong *et al* (2005) used this technique for an alumina particle mounted on an AFM cantilever against a copper surface. The results showed a significant reduction in adhesion when citric acid was present in the solution. Since the surface of copper generally tends to be negatively charged in a liquid (Jones 1996), an attractive or repulsive force would be generated if the particles were positively or negatively charged, respectively. The alumina particles were positively charged in the pH range of the slurry, but with the addition of citric acid surface charge changed from positive to negative on the particles, and the associated repulsive force led to a reduction in adhesion. It was also reported that a reduction in the macroscale friction and scratch defect counts was found on a copper surface polished with a slurry containing citric acid and alumina particles. Moreover interaction forces were examined for a silica particle mounted on an AFM tip against a silicon dioxide wafer. Increased repulsive forces were found with pH, consistent with a decrease in the macroscopic friction (Choi *et al* 2004).

Similar studies have been reported in the case of ceria based slurries. These slurries are commonly used for silicon dioxide CMP. The removal rate was found to be significantly larger than that obtained using a silica based slurry (Chandrasekaran 2004, Evans 2004). Abiade *et al* (2006) found a strong attractive force at pH 4.5 between a ceria thin film and a silicon dioxide particle attached to an AFM cantilever. They additionally examined a macroscopic friction force generated between a silicon dioxide wafer and a polishing pad in CMP with the presence of either silica based or ceria based slurry. The friction force profile showed a sharp peak at pH 4.5 for the ceria slurry, while a monotonic decrease was observed for the silica based slurry. It was concluded that the peak in the friction force occurred due to an electrostatic attraction between ceria particles and silicon dioxide on a wafer. Based on this finding, a mechanical removal process, assisted by electrostatic interactions, was hypothesized in this pH range as a primary material removal mechanism, rather than chemical reaction processes previously proposed (Evans 2004). Katsuki *et al* (2000) found equivalent molar wear volume for a silicon tip sliding against a silicon dioxide film. It was claimed that these results provided strong evidence of Si–O–Si bridge formation and its breakage during the material removal in CMP.

Sokolov *et al* (2006) used the AFM adhesion technique to estimate the surface potential of a polyurethane surface at various pHs. Polyurethane materials are typically used for polishing pads, so the interaction with silica particles is important. A similar trend was found between the surface potential and zeta potential, a macroscopic indicator of surface charging for particles.

4. Applications and future challenges for MEMS/NEMS

The success of digital micro-mirror array (DMA) systems for optical projectors as well as various sensors has accelerated the incorporation of MEMS/NEMS into practical applications (Bhushan 2007). In MEMS/NEMS, surface forces, such as adhesion and friction, become significant because of the large surface area to volume ratio. Recent studies have revealed the profound influence of adhesion, friction and wear on the efficiency, power output, steady state motion and reliability of these devices (Bhushan *et al* 2005, Bhushan 2007). CMP processes enable the modification of the surface roughness, waviness and flatness; therefore those can be incorporated in the MEMS/NEMS manufacturing process as a key step.

Compared to IC wafer applications, two distinguishing differences can be pointed out in MEMS applications versus IC wafer CMP (von Trotha *et al* 2004). (1) A relatively larger amount of material is removed. Due to the larger topographical structures used for MEMS, the removal rate required must be two to five times larger than that for IC wafers, typically 0.5 μm min^{-1}. This requirement is a challenge for MEMS CMP, while other requirements critical to IC wafers, such as dishing, erosion and roughness, may not be applicable. (2) There is a variety of materials requiring polishing. In addition to silicon oxide and metals, mainly used for IC wafers, MEMS devices employ polymers and other types of ceramics and metals.

An example of MEMS CMP is the fabrication step of a DMA system. An aluminum mirror is supported by a post made of nickel and is manipulated by an electrostatic force so that the reflected light that needs to be projected can be selected. In the fabrication process, DMAs are often made by surface machining of a copper sacrificial layer. The copper layer is later removed to form DMAs. To obtain well aligned mirrors, the copper surface on which the DMAs are deposited must be planarized, and CMP is used (von Trotha *et al* 2004). Liu and Bhushan (2004) have made a comprehensive study on the tribological issues of DMA systems. A similar CMP process applied in the planarization of a copper sacrificial layer

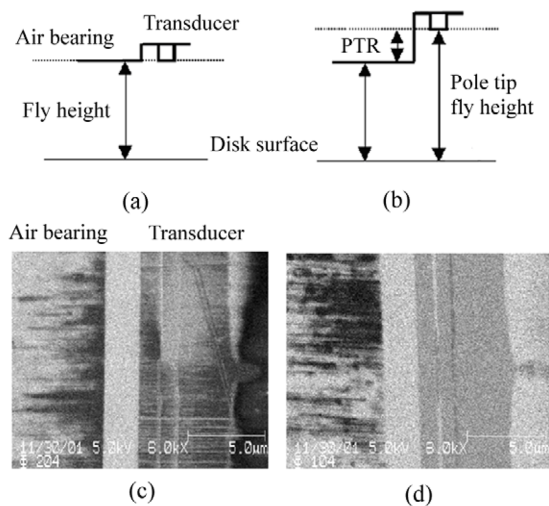

Figure 9. Illustration of (a) zero PTR and (b) regular negative PTR air-bearing sliders for hard disk drives (HDDs). Auger carbon maps are also shown for (c) zero and (d) negative PTR sliders after stressed flyability tests. Depletion of protective carbon coating is seen appearing as dark streaks owing to head/disk mechanical contact.

has also been used for the formation of RF-MEMS devices (Laborie *et al* 2006).

The planarization process achieved by CMP is also important for the fabrication of acceleration MEMS sensors. In this application, polysilicon micro-machined lateral structures are formed using lithography. The surface planarization of deposited polysilicon is a critical step prior to subsequent lithography steps in order to create repeating patterns (Bhushan 2007).

A CMP process was shown to be useful in a fabrication process for the monolithic integration of MEMS into CMOS (Eaton and Smith 1996, Kumar *et al* 2006). A pressure sensor MEMS is fabricated on a silicon substrate using CMP and is bonded with a silicon layer to which a CMOS structure is fabricated. The manufacturing process for the two different devices can be independently processed and then integrated onto the same substrate.

The fabrication of air-bearing sliders with read/write transducers for hard disk drive (HDD) systems is another important application of MEMS CMP. During CMP of air-bearing slider surfaces, the difference in the removal rate between the air-bearing material (Al–Ti–C ceramics) and the transducer material (Ni–Cr) creates a height gap called a pole tip recession (PTR) (Bhushan 1996a). Manipulation of the CMP slurry formulation allows different levels of PTR: a zero PTR slider in figure 9(a) and regular negative PTR sliders in (b). These were used in component-level fly tests in a forced environment (low pressure and high temperature). Figures 9(c) and (d) show a carbon map obtained by Auger electron microscopy (AES), revealing the wear on the air-bearing and the transducer surface. The zero PTR slider was more susceptible to transducer damage than the negative PTR slider, as indicated by the depletion of an amorphous protected carbon layer. Transducer damage can result in a serious malfunction of a HDD system.

5. Conclusion

Fundamental aspects of CMP are discussed at the macro and micro/nanoscales. Relative speeds of a wafer against a polishing pad under specific rotation speeds of a carrier and a platen are derived from a kinematic analysis and are further confirmed by the measurements of frictional force and removal rate. The Preston equation has been re-examined from the mechanistic view point and the correlation between the kinematic parameters and the removal rate was interpreted using other approaches, such as an energy balance model. Based on the kinematics and Preston's law, tribological models at the wafer/pad interface have been established to evaluate the non-uniformity in the removal rate across the wafer sample. The modeling has suggested that the wafer is most likely tilted toward the leading edge due to the frictional force, when the wafer is supported by a gimbal ball joint. Tribological approaches, i.e. contact mechanics and fluid lubrication theories were used for the analysis. In the asperity contact (micro/nano) scale, Langmuir–Hinshelwood style kinetics, which combines chemical and mechanical material removal mechanisms, has been found to be effective to elucidate the fundamental CMP processes. To experimentally verify the CMP mechanisms at the micro/nanoscale, AFM tip scratch/adhesion tests using a fluid cell have been conducted, simulating the asperity contact between a wafer and polishing pad through abrasive particles in CMP. The results indicated that microscopic observations were consistent with macroscopic phenomena, e.g. enhanced material removal rates in a slurry environment and increased adhesive forces in specific pH ranges. Finally, applications in MEMS/NEMS devices were described, which suggested that CMP techniques have become efficient for the emerging application fields.

Acknowledgments

The authors thank Edward Remsen, Yoshio Homma, Michael Lacy, Jaishankar Kasthurirangan (Cabot Microelectronics Corp.) and Leonard Borucki (Araca Inc.) for fruitful discussions and useful suggestions.

References

Abiade J T, Yeruva S, Choi W, Moudgil B M, Kumar D and Singh R K 2006 A tribological study of ceria-silica interactions for CMP *J. Electrochem. Soc.* **153** G1001–4

Ahearne E and Byrne G 2004 Ultraprecision grinding technologies in silicon semiconductor processing *Proc. Inst. Mech. Eng.* B **218** 253–67

Ahmadi G and Xia X 2001 A model for mechanical wear and abrasive particle adhesion during the chemical mechanical polishing process *J. Electrochem. Soc.* **148** G99–109

Aksu S, Wang L and Doyle F M 2003 Effect of hydrogen peroxide on oxidation of copper in CMP slurries containing glycine *J. Electrochem. Soc.* **150** G718–23

Archard J 1953 Contact and rubbing of flat surfaces *J. Appl. Phys.* **24** 981–8

Archard J 1977 Wear theory and mechanisms *The Wear Control Handbook* (New York: ASME) pp 35–80

Berdyyeva T K, Emery S B and Sokolov I Y 2003 *In situ* AFM study of surface layer removal during copper CMP *Electrochem. Solid-State Lett.* **6** G91–4

Bhushan B 1996a *Tribology and Mechanics of Magnetic Storage Systems* 2nd edn (New York: Springer)

Bhushan B 1996b Methodology for roughness measurement and contact analysis for optimization of interface roughness *IEEE Trans. Magn.* **32** 1819–25

Bhushan B (ed) 1999 *Handbook of Micro/Nanotribology* 2nd edn (Boca Raton, FL: CRC Press)

Bhushan B 2002 *Introduction to Tribology* (New York: Wiley)

Bhushan B 2005a Nanotribology and nanomechanics *Wear* **259** 1507–31

Bhushan B (ed) 2005b *Nanotribology and Nanomechanics—An Introduction* (Heidelberg: Springer)

Bhushan B (ed) 2007 *Springer Handbook of Nanotechnology* 2nd edn (Heidelberg: Springer)

Bhushan B, Kasai T, Kulik G, Barbieri L and Hoffmann P 2005 AFM study of perfluoroalkylsilane and alkylsilane self-assembled monolayers for anti-stiction in MEMS/NEMS *Ultramicroscopy* **105** 176–88

Borucki L J, Ng S H and Danyluk S 2005 Fluid pressures and pad topography in chemical mechanical polishing *J. Electrochem. Soc.* **152** G391–7

Borucki L and Philipossian A 2007 *Microelectronic Applications of Chemical–Mechanical Planarization* ed Y Li (New York: Wiley) chapter 6 (Modeling) pp 171–200

Brown N J, Baker P C and Maney R T 1981 Optical polishing of metals *Proc. SPIE* **306** 42–57

Bullen D, Scarfo A, Koch A, Bramono D P Y, Coppeta J and Racz L 2000 *In situ* technique for dynamic fluid film pressure measurement during chemical mechanical polishing *J. Electrochem. Soc.* **147** 2741–3

Castillo-Mejia D and Beaudoin S 2003 A locally relevant Prestonian model for wafer polishing *J. Electrochem. Soc.* **150** G96–102

Castillo-Mejia D, Perlov A and Beaudoin S 2000 Quantitative prediction of SiO_2 removal rates during chemical mechanical polishing *J. Electrochem. Soc.* **147** 4671–5

Chandrasekaran N 2004 Material removal mechanisms of oxide and nitride CMP with ceria and silica-based slurries *Mater. Res. Soc. Symp. Proc.* **816** K9.2

Chen L and Guay D 1994 Selected dissolution of aluminum initiated by atomic force microscope tip–surface interaction *J. Electrochem. Soc.* **141** L43–5

Choi W, Lee S-M and Singh R K 2004 pH and down load effects on silicon dioxide dielectric CMP *Electrochem. Solid-State Lett.* **7** G141–4

Cook L M 1990 Chemical process in glass polishing *J. Non-Cryst. Solids* **120** 152–71

Cooper K, Eichenlaub S, Gupta A and Beaudoin S 2002 Adhesion of aluminum particles to thin films *J. Electrochem. Soc.* **149** G239–44

DeVecchio D and Bhushan B 1998 Use of a nanoscale Kelvin probe for detecting wear precursors *Rev. Sci. Instrum.* **69** 3618–24

DeVecchio D, Schmutz P and Frankel G S 2000 A new approach for the study of chemical mechanical polishing *Electrochem. Solid-State Lett.* **3** 90–2

Eaton W P and Smith J H 1996 Planar surface-micromachined pressure sensor with a sub-surface, embedded reference pressure cavity *Micromachined Devices and Components (Austin, TX)*; *Proc. SPIE* **2882** 259–65

Evans C J, Paul E, Dornfeld D, Lucca D A, Byrne G, Tricard M, Klocke F, Dambon O and Mullany B A 2003 Material removal mechanisms in lapping and polishing *ICRP Ann.* **52** 611–33

Evans D R 2004 Cerium oxide abrasives, observations and analysis *Mater. Res. Soc. Symp. Proc.* **816** K9.1

Gray C, Rogers C, Manno V P, White R, Moinpour M and Anjur S 2007 Determining pad-wafer contact using dual emission laser induced fluorescence *Mater. Res. Soc. Symp. Proc.* **991** C1.4

Greenwood J and Williamson J 1966 Contact and nominally flat surfaces *Proc. R. Soc.* A **295** 300–19

Guo Y, Chandra A and Bastawros A-F 2004 Analytical dishing and step height reduction model for CMP with a viscoelastic pad *J. Electrochem. Soc.* **151** G583–9

Hagihara T, Naito K and Fujii S 2002 Polishing composition *US Patent Speficication* 6,454,820B2

Halley D G 2003 Spherical drive assembly for chemical mechanical planarization *US Patent Speficication* 6,511,368B1

Hamrock B J, Schmid S R and Jacobson B O 2004 *Fundamentals of Fluid Film Lubrication* (New York: Dekker)

Heilmann P and Rigney D A 1981 An energy-based model of friction and its application to coated systems *Wear* **72** 195–217

Higgs C F III, Ng S H, Borucki L, Yoon I and Danyluk S 2005 A mixed-lubrication approach to predicting CMP fluid pressure modeling and experiments *J. Electrochem. Soc.* **152** G193–8

Hinshelwood C N 2005 *The Structure of Physical Chemistry* (New York: Oxford University Press)

Hocheng H, Huang Y-L and Chen L-J 1999 Kinematic analysis and measurement of temperature rise on a pad in chemical mechanical planarization *J. Electrochem. Soc.* **146** 4236–9

Hocheng H, Tsai H Y and Su Y T 2001 Modeling and experimental analysis of the material removal rate in the chemical mechanical planarization of dielectric films and bare silicon wafers *J. Electrochem. Soc.* **148** G581–6

Homma Y 2006 Dynamical mechanism of chemical mechanical polishing analyzed to correct Preston's empirical model *J. Electrochem. Soc.* **153** G587–90

Homma Y, Fukushima K, Kondo S and Sakuma N 2003 Effects of mechanical parameters on CMP characteristics analyzed by two-dimensional friction-force measurement *J. Electrochem. Soc.* **150** G751–7

Hong Y, Han J, Song J and Park J 2005 Frictional behavior and particle adhesion of abrasive particles during Cu CMP *Mater. Res. Soc. Symp. Proc.* **867** W6.2

Hutchings I M 2002 Abrasion processes in wear and manufacturing *Proc. Inst. Mech. Eng.* J **216** 55–62

Jeng Y-R, Huang P-Y and Pan W-C 2003 Tribological analysis of CMP with partial asperity contact *J. Electrochem. Soc.* **150** G630–7

Jindal A, Li Y and Babu S V 2001 Effect of pH on chemical–mechanical polishing of copper and tantalum *Mater. Res. Soc. Symp. Proc.* **671** M6.8

Johnson K L 1985 *Contact Mechanics* (Cambridge: Cambridge University Press)

Jones D A 1996 *Principles and Prevention of Corrosion* 2nd edn (Upper Saddle River, NJ: Prentice-Hall)

Kaanta C W, Bombardier S G, Cote W J, Hill W R, Kerszykowski G, Landis H S, Poindexter D J, Polland C W, Ross G H, Ryan J G, Woff S and Cronin J E 1991 Dual damascene: a ULSI wiring technology *VLSI Multilevel Interconnection Conference (VMIC) Proc. (Santa Clara, CA)* pp 144–52

Karthikeyan S, Kim H J and Rigney D A 2005 Velocity and strain-rate profiles in materials subjected to unlubricated sliding *Phys. Rev. Lett.* **95** 106001

Kasai T 2008 A kinematic analysis of disk motion in a dual sided polisher for chemical mechanical planarization (CMP) *Tribol. Int.* **41** 111–8

Katsuki F, Kamei K, Saguchi A, Takahashi W and Watanabe J 2000 AFM studies on the difference in wear behavior between Si and SiO_2 in KOH solution *J. Electrochem. Soc.* **147** 2328–31

Kaufman F B, Thompson D B, Broadie R E, Jaso M A, Guthrie W L, Pearson D J and Small M B 1991 Chemical–mechanical polishing for fabricating patterned W metal features as chip interconnects *J. Electrochem. Soc.* **138** 3460–5

Kim A T, Seok J, Tichy J A and Cale T S 2003 A multiscale elastohydrodynamic contact model for CMP *J. Electrochem. Soc.* **150** G570–6

Kim I-K, Kang Y-J, Hong Y-K and Park J-G 2005 Effect of corrosion inhibitor (BTA) in citric acid based slurry on Cu CMP *Mater. Res. Soc. Symp. Proc.* **867** W1.3

Kim T W and Bhushan B 2006 Generation of composite surfaces with bimodal distribution and contact analysis for optimum tribological performance *ASME J. Tribol.* **128** 851–64

Kumar V V, Dasgupta A and Bhat K N 2006 Process optimization for monolithic integration of piezoresistive pressure sensor and MOSFET amplifier with SOI approach *J. Phys. Conf. Ser.* **34** 210–5

Laborie B, Souiller J, Torkler M, Huth C, Lisec T and Zwicker G 2006 Development of a custom-designed copper slurry for the fabrication of an RF-MEMS devices *ICPT Conf. Proc. (Foster City, CA)*

Lawing A S 2002 Pad conditioning and pad surface characterization in oxide chemical mechanical polishing *Mater. Res. Soc. Symp. Proc.* **732** I5.3

Lin X-Y, Creuzet F and Arribart H 1993 Atomic force microscopy for local characterization of surface acid–base properties *J. Phys. Chem.* **97** 7272–6

Liu H and Bhushan B 2004 Nanotribological characterization of digital micromirror devices using an atomic force microscope *Ultramicroscopy* **100** 391–412

Lu J, Rogers C, Manno V P, Philipossian A, Anjur S and Moinpour M 2004 Measurements of slurry film thickness and wafer drag during CMP *J. Electrochem. Soc.* **151** G241–7

Luo J and Dornfeld D A 2003 Effects of abrasive size distribution in chemical mechanical planarization: modeling and verification *IEEE Trans. Semicond. Manuf.* **16** 469–76

Luo J and Dornfeld D A 2004 *Integrated Modeling of Chemical Mechanical Planarization for Sub-Micron IC Fabrication* (Heidelberg: Springer)

Luo Q, Ramarajan S and Babu S V 1998 Modification of the Preston equation for the chemical–mechanical polishing of copper *Thin Solid Films* **335** 160–7

Ng S H, Yoon I, Higgs C F III and Danyluk S 2004 Wafer-bending measurements in CMP *J. Electrochem. Soc.* **152** G819–23

Oliver M R (ed) 2004 *Chemical Mechanical Planarization of Semiconductor Materials* (Heidelberg: Springer)

Ong Q K and Sokolov I 2007 Method of making single nanoparticle terminated tips for atomic force microscopy *J. Colloid Interface Sci.* **310** 385–90

Patri U B, Pandija S and Babu S V 2005 Role of molecular structure of complexing/chelating agents in copper CMP slurries *Mater. Res. Soc. Symp. Proc.* **867** W1.11

Patrick W J, Guthrie W L, Standley C L and Schiable P M 1991 Application of chemical mechanical polishing to the fabrication of VLSI circuit interconnections *J. Electrochem. Soc.* **138** 1778–84

Paul E 2001 Application of a CMP model to tungsten CMP *J. Electrochem. Soc.* **148** G359–63

Paul E, Kaufman F, Brusic V, Zhang J, Sun F and Vacassy R 2005 A model of copper CMP *J. Electrochem. Soc.* **152** G322–8

Paul E and Vacassy R 2003 A model of CMP, III. Inhibitors *J. Electrochem. Soc.* **150** G739–43

Preston F W 1927 The theory and design of plate glass polishing machines *J. Soc. Glass Technol.* **11** 214–56

Remsen E E, Anjur S, Boldridge D, Kamiti M, Li S, Johns T, Dowell C, Kasthurirangan J and Feeney P 2006 Analysis of large particle count in fumed silica slurries and its correlation with scratch defects generated by CMP *J. Electrochem. Soc.* **153** G453–61

Rigney D A 1988 Sliding wear of metals *Annu. Rev. Mater. Sci.* **18** 141–63

Rigney D A 1997 Comments on the sliding wear of metals *Tribol. Int.* **30** 361–7

Runnels S R 1994 Feature-scale fluid-based erosion modeling for chemical–mechanical polishing *J. Electrochem. Soc.* **141** 1900–4

Runnels S R and Eyman L M 1994 Tribology analysis of chemical–mechanical polishing *J. Electrochem. Soc.* **141** 1698–701

Scarfo A M, Manno V P, Rogers C B, Anjur S P and Moinpour M 2005 *In situ* measurement of pressure and friction during CMP of contoured wafers *J. Electrochem. Soc.* **152** G477–81

Schmutz P and Frankel G S 1998 Corrosion study of AA2024-T3 by scanning Kelvin probe force microscopy and *in situ* atomic force microscopy scratching *J. Electrochem. Soc.* **145** 2295–306

Schmutz P and Frankel G S 1999 Influence of dichromate ions on corrosion of pure aluminum and AA2024-T3 in NaCl solution studied by AFM scratching *J. Electrochem. Soc.* **146** 4461–72

Sokolov I, Ong Q K, Shodiev H, Chechik N, James D and Oliver M 2006 AFM study of forces between silica, silicon nitride and polyurethane pads *J. Colloid Interface Sci.* **300** 475–81

Steigerwald J M, Murarka S P and Gutmann R J 1997 *Chemical Mechanical Planarization of Microelectronic Materials* (New York: Wiley)

Stevens F, Langford S and Dickinson J T 2003 Single asperity chemical mechanical wear studied by atomic force microscopy *Mater. Res. Soc. Symp. Proc.* **767** F2.1

Sukharev V 2001 Fluctuation model of chemical mechanical planarization *J. Electrochem. Soc.* **148** G172–7

Sundararajan S, Thakurta D G, Schwendeman D W, Murarka S P and Gill W N 1999 Two-dimensional wafer-scale chemical mechanical planarization models based on lubrication theory and mass transport *J. Electrochem. Soc.* **146** 761–6

Thagella S, Sikder A K and Kumar A 2004 Tribological issues and modeling of removal rate of low-*k* films in CMP *J. Electrochem. Soc.* **151** G205–15

Tichy J, Levert J A, Shan L and Danyluk S 1999 Contact mechanics and lubrication hydrodynamics of chemical mechanical polishing *J. Electrochem. Soc.* **146** 1523–8

Tseng W-T, Chin J-H and Kang L-C 1999 A comparative study on the roles of velocity in the material removal rate during chemical mechanical polishing *J. Electrochem. Soc.* **146** 1952–9

Vlassak J J 2004 A model for chemical–mechanical polishing of a material surface based on contact mechanics *J. Mech. Phys. Solids* **52** 847–73

von Trotha L, Mörsch G and Zwicker G 2004 Advanced MEMS fabrication using CMP *Semicond. Int.* (Aug) 54–6

Wang D, Lee J, Holland K, Bibby T, Beaudoin S and Cale T 1997 Von Mises stress in chemical–mechanical polishing processes *J. Electrochem. Soc.* **144** 1121–7

Warnock J 1991 A two-dimensional process model for chemimechanical polish planarization *J. Electrochem. Soc.* **138** 2398–402

White D, Melvin J and Boning D 2003 Characterization and modeling of dynamic thermal behavior in CMP *J. Electrochem. Soc.* **150** G271–8

Xie Y and Bhushan B 1996a Effects of particle size, polishing pad and contact pressure in free abrasive polishing *Wear* **200** 281–95

Xie Y and Bhushan B 1996b Fundamental wear studies with magnetic particles and head cleaning agents used in magnetic tapes *Wear* **202** 3–16

Ye Y Y, Biswas R, Bastawros A and Chandra A 2003 Atomistic mechanisms underlying chemical mechanical planarization of copper *Mater. Res. Soc. Symp. Proc.* **767** K1.8

Yoshida T 2005 Multi-scale physical CMP simulation framework for ECAD *CMP-MIC Proc. (Fremont, CA)* pp 233–42

Yu T K, Yu C C and Orlowski M 1993 A statistical polishing pad model for chemical–mechanical polishing *Proc. IEEE Int. Electron Dev. Mfg* pp 865–8

Zhang F and Busnaina A 1998 The role of particle adhesion and surface deformation in chemical mechanical polishing process *Electrochem. Solid-State Lett.* **1** 184–7